PROCEEDINGS OF SCIENCE

SNO

José Maneira[*†]
LIP - Laboratório de Instrumentação e Física Experimental de Partículas
Av. Prof. Gama Pinto 2, 1649-003 Lisboa, Portugal
and
Departamento de Física, Faculdade de Ciências da Universidade de Lisboa,
Edifício C8, Campo Grande 1749-016 Lisboa, Portugal
E-mail: maneira@lip.pt

An overview of the Sudbury Neutrino Observatory is presented, starting from its motivations in the early days, up to the achievements recently recognized with the 2015 Nobel Prize in Physics and the 2016 Breakthrough Prize in Fundamental Physics, that this session of the Neutrino Telescopes Workshop celebrates. After describing the main design features, the paper will focus on the experimental challenges faced over the years, and then on the results of the three data-taking phases, including the solar neutrino combination analyses.

XVII International Workshop on Neutrino Telescopes
13-17 March 2017
Venezia, Italy

[*]Speaker.
[†]On behalf of the SNO collaboration. The author would like to thank the workshop organizers for the invitation.

PoS(NEUTEL2017)002

1. Solar Neutrinos and the early days of SNO

The pioneering solar neutrino experiment of R. Davis Jr. [1] was aimed at testing the hypothesis of nuclear reactions as the energy source powering the Sun. The first solar model based on nuclear reactions (mostly the CNO cycle) was proposed by H. Bethe in the 1930's [2]. Improvements led to recognizing a stronger role to the pp chain, and a detectable flux of the higher energy component from ^8B decay. J. Bahcall calculated [3] the flux of solar neutrinos and a neutrino detection rate for the Davis experiment that was roughly 3 times the measured one. This was the start of the solar neutrino problem, to which Gribov and Pontecorvo suggested neutrino oscillations was the solution [4].

H. Chen's idea for what would become the Sudbury Neutrino Observatory (SNO) [5] was that of a detector that could be separately sensitive to different flavors of solar neutrinos and thus make an observation of flavor change that was independent of comparisons to solar model fluxes. The use of deuterium as a detection target was key to this proposed measurement, and G. Ewan made the Canadian connection, given the availability of large quantities of heavy water, and deep mines where to host the experiment. The SNO collaboration (see Fig. 1) was formed and a proposal was made [6, 7] to build the experiment in the Creighton mine (near Sudbury, Ontario), the deepest nickel mine in Canada and one of the deepest mines in the world.

Figure 1: SNO Collaboration during the 1987 Chalk River meeting. Herb Chen and George Ewan, respectively US and Canada spokespersons since 1984, are fifth and third from the right. David Sinclair, UK spokesperson since 1985, is third from the left. Art McDonald, US spokesperson since 1987, SNO Project Director since 1990, 2015 Nobel Prize in Physics, is first from the right.

When the proposal was approved in 1990, A. B. McDonald became Project Director. He oversaw the phases of construction, commissioning, data-taking and analysis and, as is well-known, received the 2015 Nobel Prize in Physics, jointly with T. Kajita. During the SNO construction, successive experiments based on different techniques and targets (Kamiokande-II, SAGE, GALLEX, Super-Kamiokande) confirmed a deficit in the observed solar neutrino interaction rate, and underlined the need for an independent measurement of solar neutrino flavor change.

2. Detector design and construction

The use of heavy water as target allows the charged (CC) and neutral (NC) current reactions on deuterium (in addition to elastic scattering on electrons) for the detection of neutrinos:

$$\mathbf{CC}: \quad \nu_e + d \rightarrow p + p + e^- \tag{2.1}$$

$$\mathbf{NC}: \quad \nu_x + d \rightarrow p + n + \nu_x \tag{2.2}$$

$$\mathbf{ES}: \quad \nu_x + e^- \rightarrow \nu_x + e^- \tag{2.3}$$

The detector design [8] is shown in Fig. 2 (left). 1000 tonnes of heavy water are contained in a 12 m diameter vessel made of UV-transparent acrylic (AV), and surrounded by an 18 m diameter stainless steel geodesic structure (PSUP) supporting an array of 9456 8-inch Hammamatsu photo-multipliers coupled to reflectors to enhance the light coverage up to 54%. The detector is housed in a cavity containing an additional 7000 tonnes of ultra-pure water (UPW) that shield the AV from gammas and neutrons coming from the surrounding rock and the PMTs themselves. Underground construction of the detector was challenging. For instance, due to the space constraints in the mine elevator, the whole AV was built of pre-bent acrylic "bricks" that had to be bonded in situ. A picture of the detector after completion of the AV, but prior to the installation of all PMTs, is shown in Fig. 3(left).

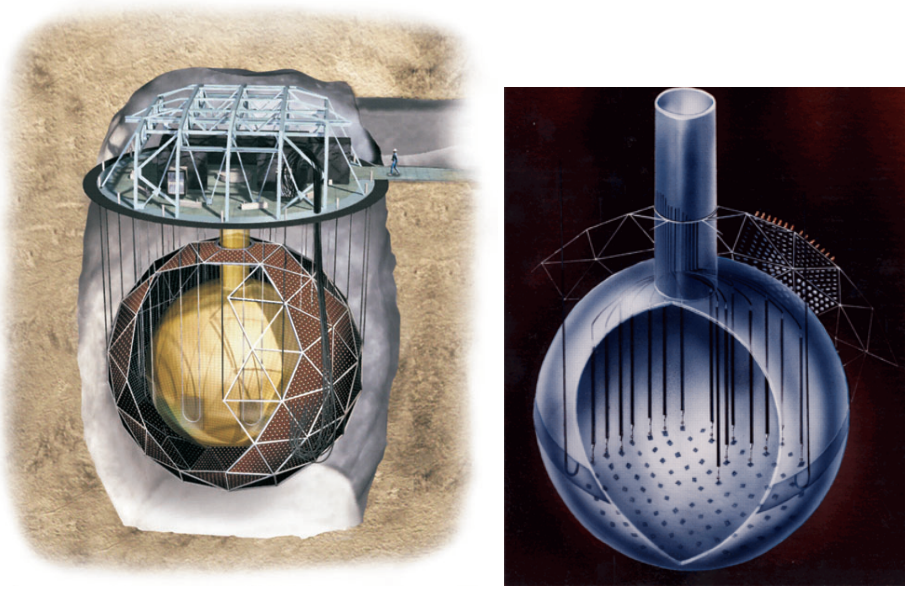

Figure 2: (left) Artist's view of the SNO Detector inside the Creighton mine experimental cavity. (right) View of SNO with the full array of ^3He proportional counters (the number of actually deployed counters was smaller than the shown 96 positions). From [10].

The detection of the free neutrons from the NC reaction is a substantial challenge, and dictated the approach of the different phases of SNO. In phase I (Nov. 1999 - May 2001), SNO observed a 6.25 MeV gamma resulting from the neutron capture by a deuteron. In phase II (June 2001 - Sept.

2003), 2 tonnes of NaCl were added to the heavy water, and SNO observed a gamma cascade with a total energy of 8.6 MeV resulting from the neutron capture by chlorine. For the third phase of SNO, an array of ^3He-filled proportional counters [9] was deployed in the heavy water, in order to provide an NC reaction observation independent of the PMT array and break any correlations between the CC and NC measurements. Fig. 2 (right) shows the SNO detector with the ^3He counter array.

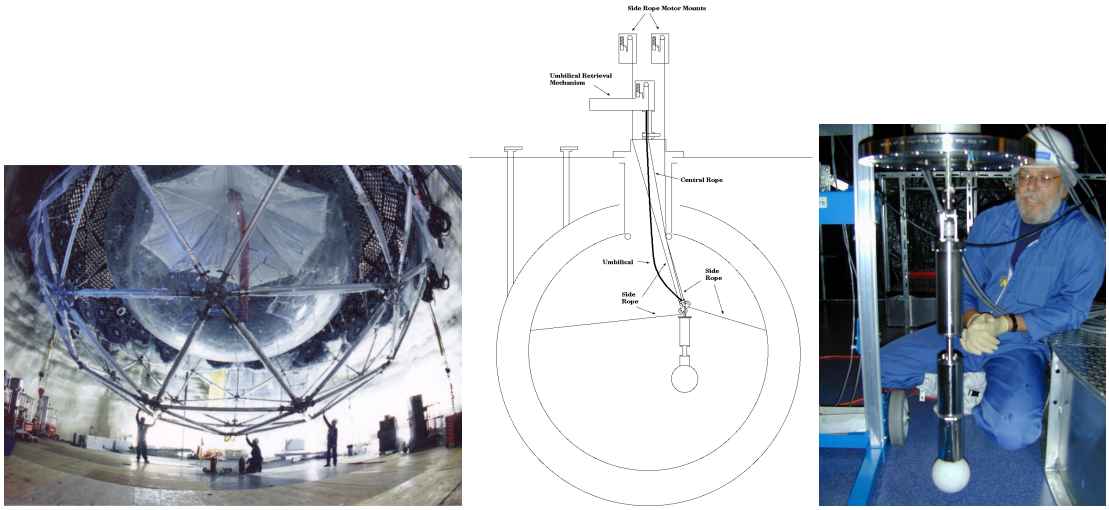

Figure 3: (left) Photo of detector construction, showing the spherical AV within the geodesic PSUP, before installing all PMT panels. (Center) Diagram showing the mechanism to move calibration sources inside the AV (not to scale). (right) Photo of the "laserball" optical calibration source, being prepared for deployment. From [10].

Another crucial part of the experiment are the systems to purify and assay the heavy water and the surrounding light water, housed in a separate cavity in the underground lab. The electronics for the PMT and NCD arrays were located just above the detector, in a purposefully built deck, the center of which houses a clean room through which several calibration sources, optical and radioactive, could be inserted inside the AV and moved in two perpendicular vertical planes (see Fig. 3 (center and right)).

3. Examples of experimental challenges

3.1 Optical calibrations

Calibrations were a very important aspect of the SNO operations, taking about 30% of the time. Several triggered radioactive sources [11, 12, 13] were deployed, of which the 6.13 MeV gamma-emitting ^{16}N was the primary monitoring tool for the energy, position and direction reconstruction, being deployed about once a month in the center of the detector. During the salt phase, a steady decrease of the average number of detected PMT hits per event (nhits) was observed the course of two years. The cause of this was tracked down to increased optical absorption in the heavy water (likely due to contamination from the radioactivity assay systems). Multi-position and multi-wavelength scans of the detector with the optical calibration source [14] (see Fig. 3, right) provided

the in-situ data to measure the attenuation coefficients of the heavy water, which were in fact observed to increase with time (see Fig. 4, left). Knowing the source of the energy response drift, it was possible to correct for it in the simulations and reconstruction (see Fig. 4, left). After all calibrations and corrections, the final uncertainty in the energy scale was below 1%.

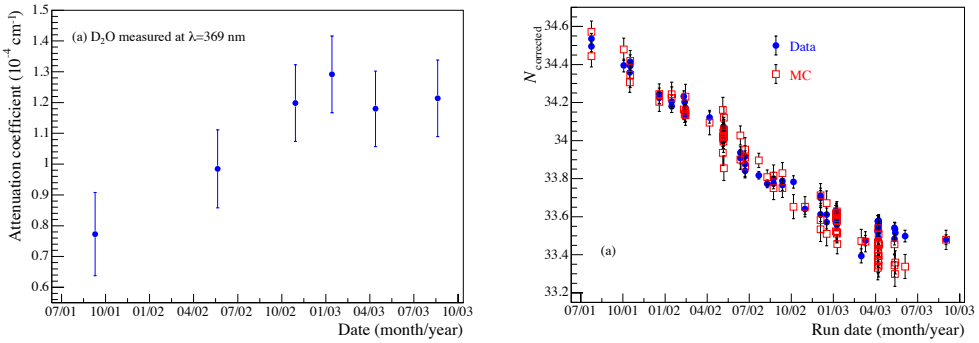

Figure 4: (left) Attenuation coefficient of the heavy water, measured in-situ in the salt phase. (right) Average number of detected PMT hits for ^{16}N calibration source events, correcting for the number of online tubes, and noise hits. The simulation represented by the MC points includes the effect of the increasing heavy water attenuation. From [20].

3.2 Neutron identification and calibration

Measuring the separate rates of the CC and NC reactions requires the capability of distinguishing the interactions of a single electron and a single neutron in a water Cherenkov detector, and also being able to constrain the neutron-producing backgrounds. This was the main reason to have three phases for the SNO data-taking mentioned earlier. In phase I, the single 6.25 MeV gamma ray would Compton scatter more than once and so, produce a fuzzier PMT hit pattern than that of a single electron. This effect was even more pronounced in the salt phase, with an 8.6 MeV cascade of gamma rays. A combination of the average of Legendre polynomials over the angles between all hit PMT pairs in an event proved to be a suitable isotropy parameter, sensitive to the differences in those classes of events, as can be seen in Fig. 5 (left).

The NC reaction rate measurement hinged directly on the knowledge of the neutron capture and detection efficiency, and this was carefully calibrated in-situ with point-like sources (AmBe and ^{252}Cf) and distributed sources from radioactivity spikes during the third phase [15]. Fig. 5 (right) shows the measured and simulated capture efficiency for neutrons coming from the ^{252}Cf source, in the first two phases. A significant increase in efficiency is visible for the salt phase, due to the higher nuclear capture cross-section in Chlorine that in Deuterium. The higher energy of the events also led to an increase in the final detection efficiency since a larger fraction of the gamma peak would remain above the (initial) 5.5 MeV energy threshold.

In the third phase the neutron detection method was significantly different, using the ^3He proportional counters. In addition to the full integrated charge, the shape of the collected pulses was also used in the analysis, namely to distinguish α background events from radioactivity in the

counters themselves. Fig. 6 (left) shows examples of pulses from αs (some counters were filled with ^4He for this purpose) and from neutrons from calibration sources.

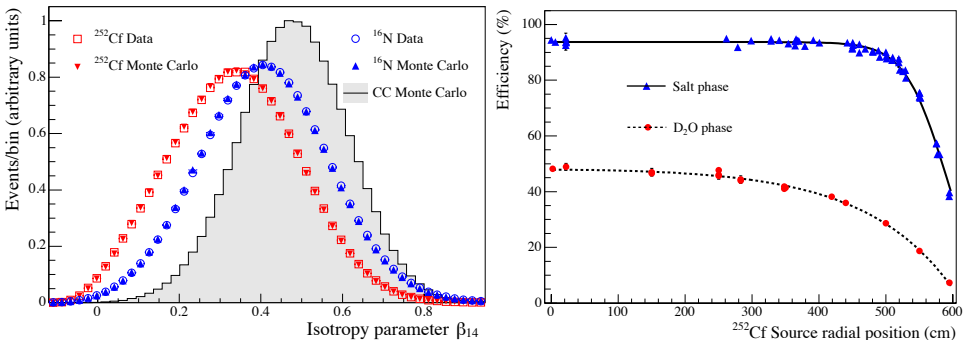

Figure 5: (left) Isotropy parameter distributions for single electron simulations (grey), single gamma calibration data and MC (blue) and neutron (multiple gammas) calibration source data and MC (red). (right) Measured and simulated capture efficiency for neutrons coming from the ^{252}Cf source. From [19, 20].

3.3 Background reduction

Radioactivity contamination in the heavy and light water, as well as in the ^3He proportional counters deployed in phase 3, caused background events in SNO. Cherenkov emission from the highest energy $\beta - \gamma$ decays of the U and Th natural chains caused backgrounds that dominated the low energy region, below 4.5 MeV. In addition photo-disintegration of deuterium produced free neutrons that were the main background to the NC rate measurement. These could only be kept small by keeping the radioactivity levels in the water low, which was achieved through the careful material selection of the detector parts, regular water purification campaigns, and careful procedures for calibration source deployment, to avoid introducing extra contamination. The radioactivity levels of three isotopes – ^{222}Rn, ^{224}Th and ^{226}Ra – were regularly monitored with two assay systems [16, 17]. The measurements, shown in Fig. 6 (right) for the heavy water, were below the target levels for almost the full data-set, with the exception of the initial phase, and deliberate ^{222}Rn injections for calibration purposes.

4. Solar Neutrino Results

SNO took data from 1999 to 2006, collecting a live-time of 277.3 days in phase 1, 391.4 days in phase 2 and 385.2 days in phase 3 (as mentioned earlier, about 30 % of data-taking time was used in calibrations). The signal-loss due to instrumental background cuts was at the level of 2% or better.

4.1 Solution of the Solar Neutrino Problem

The signal extraction method employed in the initial analyses of the first and second phases compared the radial position, direction (with respect to the Sun) and isotropy parameters of the candidate events to template distributions for CC, NC, ES and backgrounds in order to obtain rate

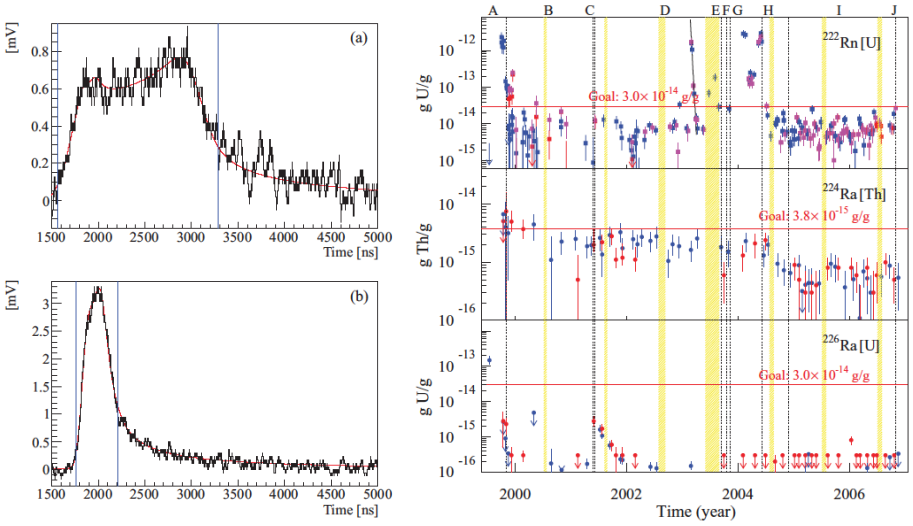

Figure 6: (left) Pulse shape examples for neutron (a) and α (b) events in the SNO ^3He proportional counters deployed in phase 3. (right) Measured activity levels of ^{222}Rn, ^{224}Th and ^{226}Ra in the SNO heavy water. From [23, 24].

measurements for each of those categories, separately for each phase. As shown in Fig. 5 (left), the isotropy distribution distinguishes between CC/ES and neutron (NC+backgrounds) events. The direction distribution allows a good separation of the ES events, and CC events to a lesser extent, due to a small anti-correlation between the electron and neutrino directions. The radial position distribution provides a good constraint on external backgrounds, and has some sensitivity to neutrons, especially in phase 1, as can be seen in Fig. 5 (right).

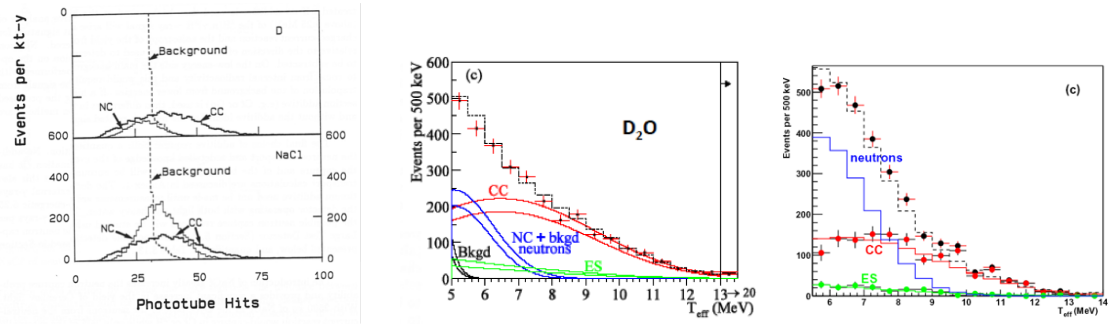

Figure 7: (left) Energy spectra predicted in the SNO proposal, and (right) measured in the first and second phases. From [7, 18, 19].

Since neutrino oscillations affect the CC and ES energy spectra, they were not used in the extraction in order to avoid a bias, but were obtained as a product of the analysis. Fig. 7 shows the energy spectra predicted in the SNO proposal (Left), and measured in the first and second phases (right). The ^8B solar neutrino fluxes measured with each reaction can be found in Refs. [18, 19, 20, 21]. The most significant results were that, while the NC measurement agreed with

solar model predictions, the CC/NC ratio was about 1/3, simultaneously proving solar neutrino flavor change and confirming the solar model calculations.

Fig. 8 (left) shows the results of phase 2 as a function of electron-neutrino flux (xx) and other-flavor neutrino flux (yy). Each reaction determines a band, and both CC, NC and ES measurements are consistent with each other assuming flavor transformation. The precision of the NC measurement increased in phases 2 and 3, as can be seen in Fig. 8 (right), and all 3 measurements were compatible with each other and with the solar model.

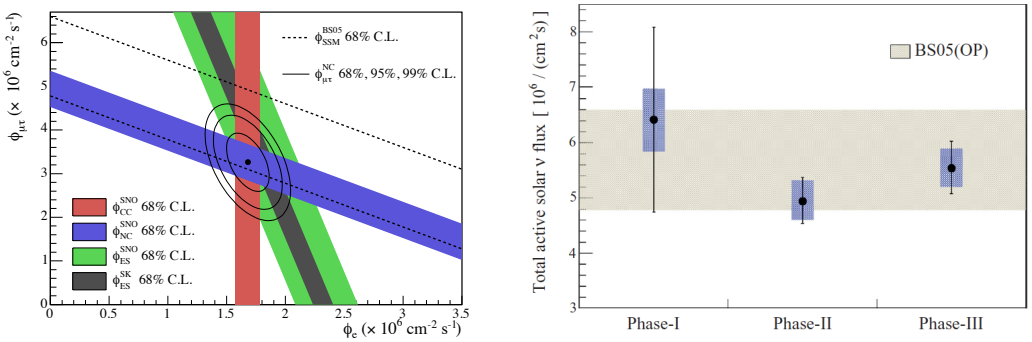

Figure 8: (left) Bands in neutrino-flavor space determined by the NC, CC and ES solar neutrino flux measurements in SNO's phase 2. (right) NC flux measurements in all 3 phases, compared to the solar model. From [20, 23].

4.2 Aiming for precision with all phases combined

Within the context of neutrino oscillations, the next main scientific goals of SNO were to increase the precision of the flux measurements, crucial for the precision of the θ_{12} mixing angle, and to look for spectral distortions, that would show the MSW character of solar neutrino oscillations. In order to accomplish that, significant improvements were implemented in the energy reconstruction and calibration, leading to a better energy resolution and consequently smaller backgrounds in the low energy region. This allowed a lower energy threshold of 3.5 MeV (w/r to 5.5 MeV in previous analyses) and a better detection efficiency for neutrons. The signal extraction method was also overhauled and was a based on a combined analysis of the first and second phases [22] (and later also the third phase [24]) in which, instead of measuring CC, NC, ES electron-neutrino-equivalent fluxes independently for each phase, the only free parameters were the flux of ^8B solar neutrinos, and a parametrization of the electron-neutrino survival probability. This allowed for a better accounting of correlated systematic uncertainties across phases.

Fig. 9 shows the measured ^8B solar neutrino flux, for which the experimental precision is significantly better than the theoretical predictions (also shown), and the measured electron-neutrino survival probability. In this latter case, with a small expected spectral distortion, the data is compatible both with the LMA hypothesis and with a flat survival probability. The increased precision of these results was carried into the oscillation parameters, by means of a 3-flavor oscillation analysis including all the solar neutrino results, as well as the KamLAND (and short baseline experiments) reactor neutrino results. The results are presented in Fig. 10, showing the complementarity be-

tween solar and KamLAND reactor data in the 12 sector, and also an early tension between solar and KamLAND due to the non-zero value of θ_{13}, that would later be measured precisely by several experiments (Daya Bay, RENO, Double Chooz, T2K, MINOS).

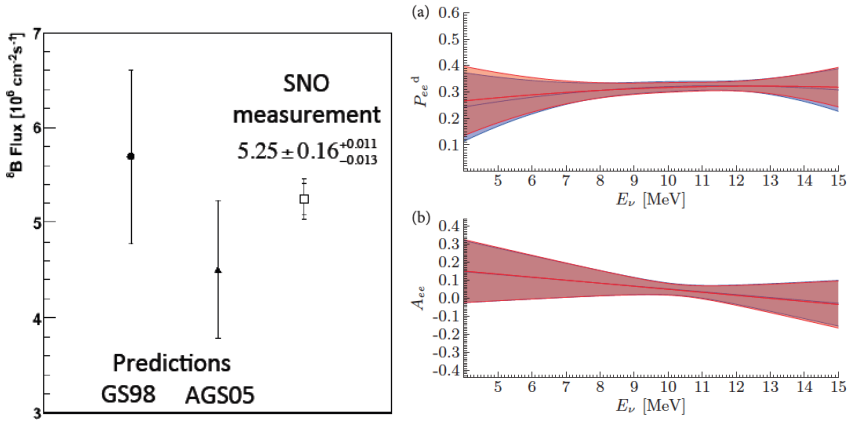

Figure 9: Measurements with the 3 phases of SNO: (Left) ^8B solar neutrino flux. (Right) Parametrized form of the electron-neutrino survival probability (top) and day-night asymmetry (bottom). From [24].

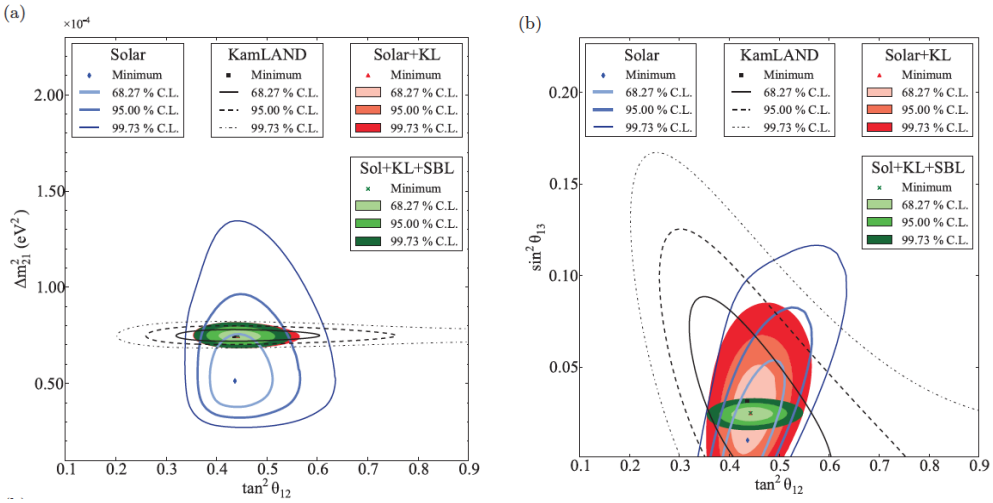

Figure 10: Results of the neutrino oscillation analysis of the SNO data combined with all other solar neutrino data, plus the KamLAND (and short baseline) reactor neutrino results. From [24].

4.3 Conclusions and Outlook

SNO was designed for and succeeded in solving the Solar Neutrino Problem, proving that neutrinos do change flavor and contributing, through a careful understanding of the detector, to precision results contributing to accurate neutrino oscillation parameters. The field of neutrino physics is now wide open to new experiments, aiming to measure CP violation, determine the absolute neutrino mass and ordering and showing whether neutrinos are or not Majorana particles.

The SNO detector is now in use as the SNO+ experiment, that will load the AV with 780 tonnes of LAB liquid scintillator loaded with 3.9 tonnes of natural Tellurium for a high-mass, low-background experiment [25] searching for the neutrino-less double-beta decay of ^{130}Te, with an expected 90% C.L. half-life sensitivity of 2×10^{26} yr, after 5 years of data-taking. SNO+ is currently taking data with water, and scintillator fill will start soon, followed by the Tellurium loading. In addition to double-beta decay, SNO+ will also be sensitive to neutrinos from the Sun, the Earth and Supernovae, as well as reactor neutrinos.

References

[1] R. Davis, Phys. Rev. Lett. 11, vol. 12 (1964), p. 303

[2] H. Bethe, Phys. Rev. vol. 55 (1939), p. 434

[3] J. Bahcall, Phys. Rev. Lett. 11, vol. 12 (1964), p. 300

[4] V. Gribov, B. Pontecorvo, Phy. Lett. B 7, vol. 28 (1969), p. 493

[5] H.H. Chen, Phys. Rev. Lett. 55, vol. 14 (1985), p. 1534

[6] D. Sinclair et al., Il Nuovo Cimento C (1986) 9: 308

[7] G.T. Ewan et al., "Sudbury Neutrino Observatory Proposal" (1987) SNO-1987-12

[8] SNO Collab., NIM A449 (2000) pp. 172-207

[9] J.F. Amsbaugh et al, NIM A579 (2007) 1054-1080

[10] SNO website: https://sno.phy.queensu.ca/sno/images/

[11] M.R. Dragowsky et al, NIMA481 (2002) 284-296

[12] A.W.P. Poon et al, NIM A452 (2000)15-129

[13] N. Tagg et. al., NIM A489 (2002) 92-102

[14] B.A. Moffat et al, NIMA554 (2005) 255-265

[15] K. Boudjemline et al, NIMA 620 (2010) 171-181

[16] T.C. Andersen et al, NIM A501 (2003) 386-398 and 399-417

[17] B. Aharmim et al, NIM A604 (2009) 531-535

[18] SNO Collab., PRL 89, 011301 (2002)

[19] SNO Collab., PRL92, 181301 (2004)

[20] SNO Collab., PRC 72, 055502 (2005)

[21] SNO Collab., PRC 75 045502 (2007)

[22] SNO Collab., PRC 81, 055504 (2010)

[23] SNO Collab., PRC 87, 015502 (2013)

[24] SNO Collab., PRC 88, 025501 (2013)

[25] SNO+ Collab., Adv. High En. Phys. vol. 2016, 6194250 (2016)